

Enhanced spreading in continuous-time quantum walks using aperiodic temporal modulation of defects

J. J. Ximenes^{1,*}, M. A. Pires^{2,†} and J. M. Villas-Bôas^{1,‡}

¹*Instituto de Física, Universidade Federal de Uberlândia, 38400-902 Uberlândia-MG, Brazil*

²*Centro Brasileiro de Pesquisas Físicas, Rio de Janeiro - RJ, 22290-180, Brazil*

Parrondo's paradox, where the alternation of two losing strategies can produce a winning outcome, has recently been demonstrated in continuous-time quantum walks (CTQWs) through periodic defect modulation. We extend this phenomenon to aperiodic protocols. We show that deterministic, non-repetitive defect switching can enhance quantum spreading in CTQWs compared to the defect-free case. Furthermore, we establish that the degree of this enhancement is strongly influenced by the autocorrelation and persistence characteristics of the applied aperiodic sequence. Our findings indicate that aperiodic defect modulation reliably maintains Parrondo's effect and provides new ways to control wavepacket properties in CTQWs.

CONTENTS

I. Introduction	1
II. Model	2
A. Continuous-time quantum walks	2
B. Switching protocols	3
III. Results and discussion	3
IV. Final remarks	5
Acknowledgments	5
References	5
A. Some exacts results for the binary persistence	7
1. Periodic sequence	7
2. Random sequence	7
B. Extra results	7

I. INTRODUCTION

The genesis of quantum walks can be traced back to the decade of the 1990s, with the introduction of two primary formulations: the discrete-time quantum walk (DTQW) and the continuous-time quantum walk (CTQW). The DTQW, formally introduced in 1993 by extending the classical random walk to the quantum realm [1], proceeds in discrete time steps governed by the application of the coin and translation operators. Subsequently, in 1998, the CTQW was also introduced [1]. The CTQW evolves continuously in time under the influence of a Hamiltonian operator. The scientific interest in QWs is sustained by the various physical realizations [2], and by the ever-increasing range of applications [3–7].

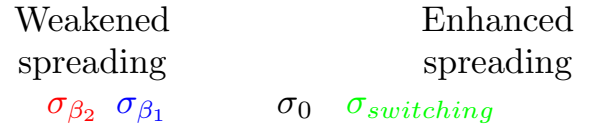


FIG. 1. Illustration of the Parrondo's paradox in the realm of CTQWs that are subject to defects. To quantify the spreading of the CTQW, we compute the standard deviation, σ , of the wavepacket probability distribution. Relative to the defect-free baseline (σ_0), spreading is classified as slow ($\sigma < \sigma_0$) or fast ($\sigma > \sigma_0$). The introduction of defects typically leads to a decrease in the spreading of the CTQW, exemplified by $\sigma_{\beta_1} < \sigma_0$ (slow) and $\sigma_{\beta_2} < \sigma_0$ (slow), representing the dynamics with a single transition defect. Surprisingly, proper temporal switching between β_1 and β_2 can lead to enhanced spreading, $\sigma_s > \sigma_0$ (fast). That is, the alternating of two unfavorable setups, can lead to favorable scenarios. This manifestation is termed the “slow+slow→ fast” effect.

In parallel to the development of quantum walks, the field of game theory witnessed the emergence of intriguing phenomena such as the Parrondo's Paradox, first formalized in 1999 [8]. In this counterintuitive phenomenon two losing games can surprisingly yield a gain when played in an alternating way. Parrondo's Paradox has since been explored in various areas of science [9, 10].

The intersection of these two aforementioned domains has been explored with several protocols for obtaining Parrondo-like effects in QWs [11–32]. But all of these earlier quantum manifestations of Parrondo's paradox have been formulated within the framework of the DTQW. Recently, in Ref. [33], Parrondo's Paradox was introduced to the domain of CTQWs. In such article the authors have focused on periodic alternations of defects. Here we investigate, for the first time, how the application of aperiodically modulated defects can induce this paradoxical phenomenon in CTQWs.

As illustrated in Fig. 1 the Parrondo's Paradox in

* jeffersonximenes@ufu.br

† piresma@cbpf.br

‡ boas@ufu.br

CTQWs emerges when we detect [33]:

$$\sigma_{\beta_1} < \sigma_0 \quad (1)$$

$$\sigma_{\beta_2} < \sigma_0 \quad (2)$$

$$\sigma_{\text{switching}} > \sigma_0 \quad (3)$$

Beyond conventional periodic order, systems displaying nontrivial arrangements, such as aperiodic sequences [34], possess wide-ranging implications in several fields such as condensed matter physics and chemistry [35] as well in non-equilibrium phenomena [36–38], stochastic game theory [39, 40] and quantum walks [41–47].

The manuscript is organized as follows: in Sect. II we describe our model designed to incorporate aperiodic defect alternation; In Sec. III we present and discuss the results for our mathematically-designed physical system; and in Sec. IV we offer final remarks on the broader significance of our findings. As we will show, the core contributions of this paper are threefold:

- (i) We establish a novel application of aperiodic sequences within quantum systems, specifically for defect modulation in CTQWs.
- (ii) We show that the Parrondo effect in CTQWs is robust and extends beyond periodic protocols to include aperiodic defect modulation.
- (iii) Our findings reveal that the structural properties of aperiodic sequences (e.g., autocorrelation, persistence) directly influence quantum transport, offering a new avenue for precisely engineering spreading and delocalization in CTQWs.

II. MODEL

A. Continuous-time quantum walks

The system consists of CTQW for a single particle on a one-dimensional lattice with two nonperiodic alternating transition defects. The model presented here extends the model developed in [33]. Hence, we first define the Hamiltonian of defect-free QW, which propagates over sites $|j\rangle$, as

$$H_0 = \epsilon \sum_j |j\rangle\langle j| - \gamma \sum_j (|j+1\rangle\langle j| + |j-1\rangle\langle j|), \quad (4)$$

with ϵ as the constant potential energy and γ as the transition rate. For the purposes of this article, we set $\epsilon = 0$, all the other variables are expressed in terms of γ . As also done by Li and Wang [48], the term for additional defect transition for nearest neighbors of site $j = d$ is defined as

$$H_d = -(|d\rangle\langle d+1| + |d+1\rangle\langle d| + |d-1\rangle\langle d| + |d\rangle\langle d-1|). \quad (5)$$

To alternate the defect intensities over time it is defined a time-dependent function, $f(t)$. The defect intensity function $f(t)$ is defined through a binary control sequence $\{s_n\}$, where $s_n \in \{0, 1\}$ denotes the state at time step n . The sequences used here are constructed as described in subsection II B. The mapping to defect intensities is given by:

$$f(t) = \begin{cases} \beta_1 & \text{if } s_{\lfloor t/\tau \rfloor} = 1 \\ \beta_2 & \text{if } s_{\lfloor t/\tau \rfloor} = 0 \end{cases} \quad \text{for } t \in \mathbb{R}^+ \quad (6)$$

where $\lfloor \cdot \rfloor$ denotes the floor function, $\tau > 0$ is the switching interval duration, and β_1 and β_2 are the defect intensities. This formulation establishes that at $t = n\tau$, the system switches defect intensity, during each interval $t \in [n\tau, (n+1)\tau)$, the defect intensity remains constant and the sequence index $n = \lfloor t/\tau \rfloor$ advances at each switching time.

Hence, in contrast to the work in [33], this time function is nonperiodic. Therefore, the Hamiltonian of this model is

$$H = H_0 + f(t)H_d. \quad (7)$$

Following [33], we take $\beta_1 = -2.5\gamma$ and $\beta_2 = -3\gamma$, that degrade the spreading, despite the observed phenomena can also be achieved for other values of defect intensities. We define without loss the generality $d = 0$.

Consequently, the state of the particle at time $|\Psi(t)\rangle$, given the initial state, is obtained from equation

$$i \frac{\partial}{\partial t} |\Psi(t)\rangle = H_0 |\Psi(t)\rangle, \quad (8)$$

where we set $\hbar = 1$. Thus, the probability distribution is obtained from $P_j(t) = |\langle j | \psi(t) \rangle|^2$. From this, we calculate the standard deviation,

$$\sigma = \sqrt{\overline{j^2} - \bar{j}^2}, \quad (9)$$

where

$$\bar{j}^n = \sum_j j^n P_j \quad (10)$$

In addition, we measure the Shannon entropy,

$$S = - \sum_j P_j \log_{10} P_j, \quad (11)$$

and, inverse participation ratio (IPR),

$$IPR = \left(\sum_j P_j^2 \right)^{-1}, \quad (12)$$

that are monotonically increasing from $S = 0$ and $IPR = 1$ (wavepacket fully localized) to $S = \log_{10} N$ and $IPR = N$ (wavepacket entirely distributed) for a wavepacket distributed over a lattice of N sites.

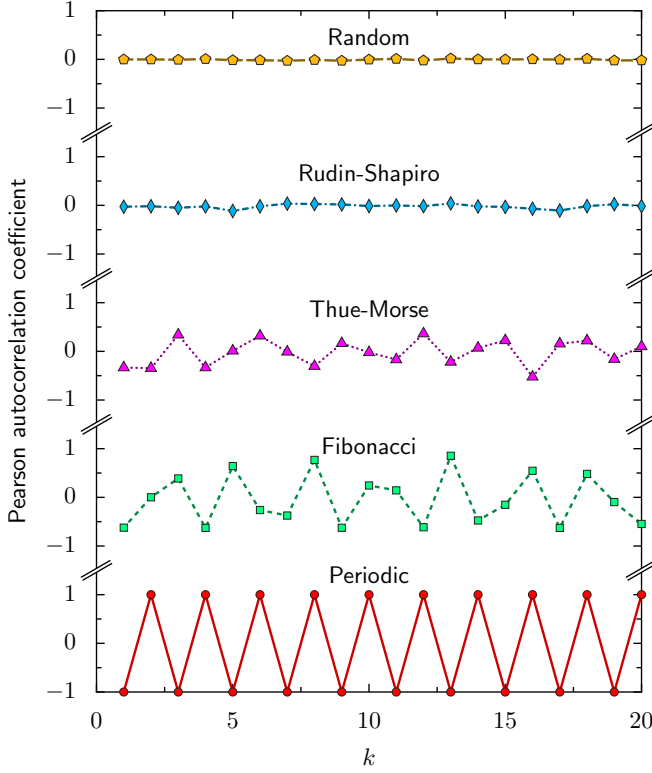


FIG. 2. Characterization of the binary sequences with the Pearson autocorrelation coefficient (AC) for a given lag k .

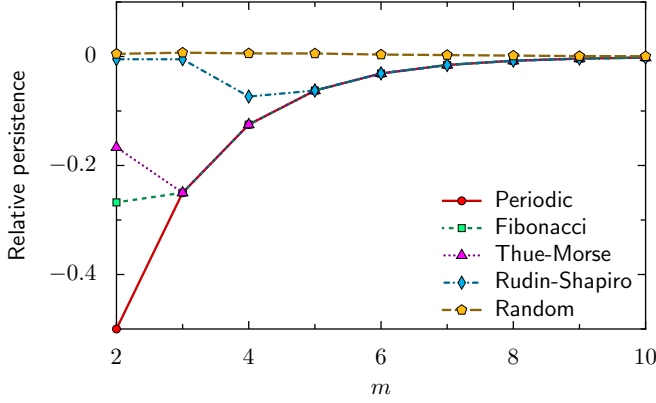


FIG. 3. Characterization of the binary sequences with the relative persistence (RP) for a given block size m .

B. Switching protocols

In line with the standard literature of binary sequences [49, 50] we generate our aperiodic sequences with the substitution rules:

1. Fibonacci (**Fb**): $w^{(0)} = 0$; $0 \mapsto 01$, $1 \mapsto 0$;
2. Thue-Morse (**TM**): $w^{(0)} = 0$; $0 \mapsto 01$, $1 \mapsto 10$;
3. Rudin-Shapiro (**RS**): $w^{(0)} = A$; $A \mapsto AB$, $B \mapsto AC$, $C \mapsto DB$, $D \mapsto DC$; Binary conversion:

$$A, B \rightarrow 0, C, D \rightarrow 1.$$

We adopt the abbreviations Pe and Rd to represent the periodic and random protocols, respectively.

To characterize the binary sequences, we computed two measures.

First, we compute the Pearson autocorrelation coefficient for a given temporal lag l

$$AC(k) = \frac{\text{Cov}(x_t, x_{t+k})}{\text{Var}(x_t)\text{Var}(x_{t+k})} \quad (13)$$

where $\text{Var}(z)$ is the variance of the variable z and $\text{Cov}(x_t, x_{t+k})$ is the covariance between x_t and x_{t+k} .

Following Ref. [40], we first compute the binary persistence of order m given by

$$BP(m) = \frac{N_{\text{ID}}(m)}{N_{\text{T}}(m)} \quad (14)$$

where $N_{\text{ID}}(m)$ is the number of blocks where all elements are identical and $N_{\text{T}}(m)$ is the total number of blocks examined. That is, $BP(m)$ computes the probability of observing a subsequence of length m consisting entirely of zeros or ones. For instance, $BP(3)$ corresponds to the proportion of subsequences 000 or 111 among all possible consecutive triplets in the sequence. In Appendix A we provide exact results for the periodic and random sequences.

As a baseline reference we consider the random sequence. Then we compute the relative binary persistence

$$RP(m) = BP(m) - 2^{1-m} \quad (15)$$

This quantity captures the nontrivial deviation from randomness and has a clear interpretation: (a) $RP > 0$ means a tendency to persistence of values, (b) $RP = 0$ means no persistence of patterns, (c) $RP < 0$ means an anti-persistent behavior, where the values tend to alternate frequently.

Figures 2 and 3 illustrate a clear hierarchy in terms of overall autocorrelation and binary persistence as indicated by

$$|AC_{Pe}| > |AC_{Fb}| > |AC_{TM}| > |AC_{RS}| \approx |AC_{Rd}| \quad (16)$$

$$|RP_{Pe}| > |RP_{Fb}| > |RP_{TM}| > |RP_{RS}| > |RP_{Rd}| \quad (17)$$

The negative values for AC and RP means a propensity for a switching of values.

Note that autocorrelation alone is not a sufficient discriminator for these sequences, underscoring the importance of the complementary measure RP .

III. RESULTS AND DISCUSSION

In this section we present our finding regarding our model that bridges Parrondo's Paradox, CTQWs and aperiodic design of defect modulation.

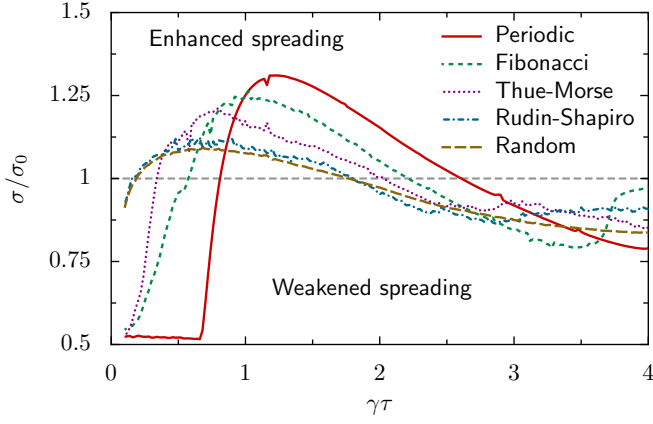


FIG. 4. Relative standard deviation σ/σ_0 as a function of τ . The point corresponds to dynamics evolution for $t = 2000\gamma$. Each point on the random case curve represents the mean of 50 random sequences, therefore, the point number is smaller than that of the aperiodic deterministic curves. The enhanced spreading zone is separated by a horizontal dashed line from reduced spreading. Note that there is an optimal switching interval, $\tau^{\min} < \tau < \tau^{\max}$, where defect modulation leads to the Parrondo's paradox in the form "slow+slow \rightarrow fast". Also note that the aperiodic protocol curves are not just a mere vertical shift of the periodic protocol curve.

Figure 4 shows that the Parrondo's effect in the CTQW is not restricted to periodic protocol, but it robustly remains in the aperiodic setting. This figure reveals the regions where the presence of these alternating defects leads to an enhancement of quantum spreading ($\sigma > \sigma_0$) and other regions where the spreading is reduced ($\sigma < \sigma_0$). In all cases the occurrence of such phenomenon is non-monotonic with τ , size of the switching interval. That is there exists a range $\tau^{\min} < \tau < \tau^{\max}$ for detection of the paradoxical behavior. Outside this interval, when τ is either too short ($\tau < \tau^{\min}$) or too long ($\tau > \tau^{\max}$), the phenomenon disappears. This suggests that the system requires sufficient time in each defect state to manifest the behavior, but not so much that the switching become negligible. For $\tau \in [\tau^{\min}, \tau^{\max}]$ there is a maximum such that

$$\sigma_{Pe}^{max} > \sigma_{Fb}^{max} > \sigma_{TM}^{max} > \sigma_{RS}^{max} > \bar{\sigma}_{Rd}^{max} \quad (18)$$

which is in accordance with the hierarchy of autocorrelation and persistence previously described.

In order to better understanding the observed phenomena let us take a look at the temporal properties of our proposed model.

Figure 5 illustrates the time evolution of the standard deviation of the wavepacket's position. The results clearly indicate that in the long-time

$$\sigma_{Pe} > \sigma_{Fb} > \sigma_{TM} > \sigma_{RS} > \bar{\sigma}_{Rd}. \quad (19)$$

This ordering is also consistent with the hierarchical values for the autocorrelation and persistence. While the transient behavior displays different local slopes, we

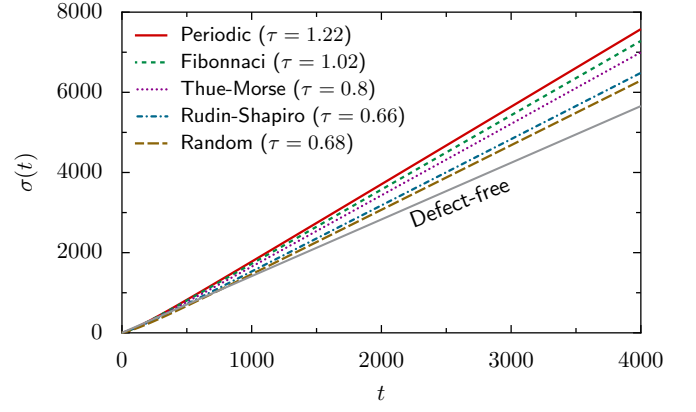


FIG. 5. Time evolution of the standard deviation for the defect-free case, along with periodic and aperiodic alternation between two defect values. The values of τ used here correspond to the maxima for each sequence in Fig. 4.

consistently observe the preservation of the ballistic-like regime in the long-run for all protocols we analyzed.

Figures 6 and 7 illustrate the complementary aspects of delocalization through the Shannon entropy (S) and inverse participation ratio (IPR). These measures reveal an important trade-off: typically protocols yielding higher spatial spreading (larger σ) correlate with lower entropy values (indicating less uniform probability distributions) and lower IPR values (signifying increased probability concentration at fewer sites).

This inverse relationship shows that enhanced spatial spreading under defect modulation comes with structured probability distributions rather than uniform delocalization. Despite their different mathematical formulations (S has logarithmic dependence while IPR has quadratic dependence), both measures consistently show the same hierarchy in the long-time limit:

$$S_{Pe} < S_{Fb} < S_{TM} < S_{RS} < \bar{S}_{Rd} \quad (20)$$

$$IPR_{Pe} < IPR_{Fb} < IPR_{TM} < IPR_{RS} < \overline{IPR}_{Rd}. \quad (21)$$

That is, aperiodic defect modulation produces intermediate levels of delocalization situated between the corresponding results for the defect-free and periodic arrangements, with both entropy and IPR capturing the same hierarchical ordering as the spatial spreading.

In a unified perspective, the results of spreading (quantified by σ) and delocalization (quantified by S and IPR) indicate that the modulation of aperiodic defects maintains Parrondo's paradox and yields tunable spreading and delocalization, placed between defect-free and periodic arrangements. This intermediate behavior can be explained through the intermediate arrangement properties of the aperiodic sequences (quantified by the autocorrelation and binary persistence). In Appendix B we add additional results that complement our findings.

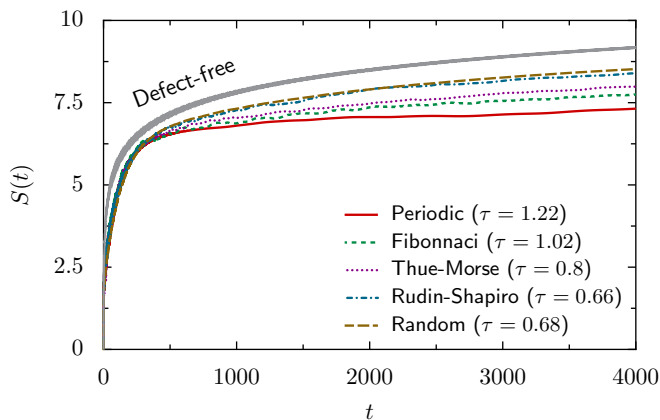


FIG. 6. Time evolution of the Shannon entropy for the evolutions in Fig. 5. At $t = 4000\gamma$, higher spatial spreading (larger σ) correlates with lower entropy values, signifying a less uniform probability distribution despite the broader spatial extent.

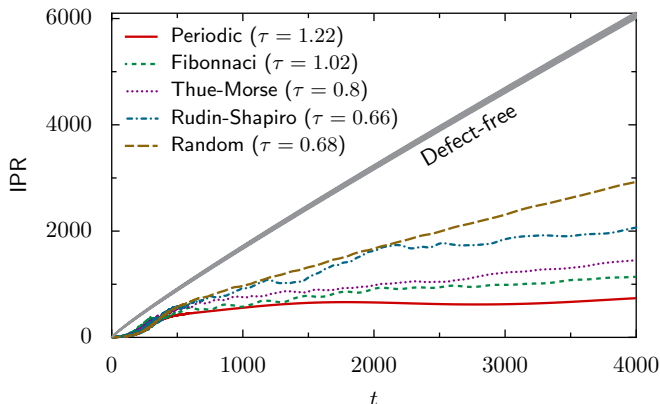


FIG. 7. Time evolution of the inverse participation ratio (IPR) for the evolutions in Fig. 5. At $t = 4000\gamma$, higher spatial spreading (larger σ) correlates with lower IPR values, indicating increased probability concentration at fewer sites despite broader spatial distribution.

IV. FINAL REMARKS

Different from previous related work that analyzed defects in QWs [51–60], we uncover that proper aperi-

odic temporal modulation of defects can induce a Parrondo phenomenon in continuous-time quantum walks (CTQWs), manifesting as a “slow + slow \rightarrow fast” effect. In this way, we go beyond the recent work [33] by showing that this counterintuitive effect is not restricted to periodic switching protocols, but it is more general and can appear in non-repetitive and structured temporal modulations of defects.

Our findings reveal that the enhancement of quantum spreading is deeply connected with the autocorrelation and persistence properties of the underlying aperiodic protocol. These results align with previous literature showing that the nontrivial properties of the aperiodic sequences can lead to interesting phenomena such as enhancement of the capital gain in alternating classical games [40], novel routes to superdiffusion in DTQWs [46], distinctive electronic [61] and thermal [62] properties.

From an implementation perspective, our deterministic protocols offer significant advantages: They avoid the statistical sampling requirements of random protocols while maintaining precise control over wavepacket properties. This makes them particularly suitable for experimental realization in quantum platforms.

In a recent review [62] it was highlighted how mathematical sequences can be leveraged to engineer materials with tailored thermal features. Building on the concept of mathematically inspired design in physical systems, we present a novel application of binary aperiodic sequences (Fibonacci, Thue-Morse, and Rudin-Shapiro) to control transport in CTQWs.

In future research endeavors, we will explore the development of protocols capable of controlling the scaling dynamics from slower-than-ballistic to faster-than-ballistic regimes. This has been achieved for DTQWs [63], but remains a challenge for CTQWs.

ACKNOWLEDGMENTS

Two of us (J. J. X and J. M. V. B.) would like to thank FAPEMIG for the financial support

-
- [1] E. Farhi and S. Gutmann, Quantum computation and decision trees, *Phys. Rev. A* **58**, 915 (1998).
 - [2] J. Wang and K. Manouchehri, *Physical implementation of quantum walks* (Springer, 2013).
 - [3] R. Portugal, *Quantum walks and search algorithms* (Springer, 2013).
 - [4] K. Kadian, S. Garhwal, and A. Kumar, Quantum walk and its application domains: A systematic review, *Computer Science Review* **41**, 100419 (2021).
 - [5] O. Mülken and A. Blumen, Continuous-time quantum walks: Models for coherent transport on complex networks, *Physics Reports* **502**, 37 (2011).
 - [6] A. Khalilipour, M. Ghorbani, and M. Arezoomand, A review on perfect, pretty good, state transfers and their applications, *Journal of Discrete Mathematics and Its Applications* **10**, 87 (2025).
 - [7] E. Desdentado, C. Calero, M. Moraga, and F. García, Quantum computing software solutions, technologies, evaluation and limitations: a systematic mapping study, *Computing* **107**, 1 (2025).
 - [8] G. P. Harmer and D. Abbott, Losing strategies can win by parrondo’s paradox, *Nature* **402**, 864 (1999).

- [9] D. Abbott, Asymmetry and disorder: A decade of parrondo's paradox, *Fluctuation and Noise Letters* **9**, 129 (2010).
- [10] T. Wen and K. H. Cheong, Parrondo's paradox reveals counterintuitive wins in biology and decision making in society, *Physics of Life Reviews* <https://doi.org/10.1016/j.plrev.2024.08.002> (2024).
- [11] A. P. Flitney, D. Abbott, and N. F. Johnson, Quantum walks with history dependence, *Journal of Physics A: Mathematical and General* **37**, 7581 (2004).
- [12] J. Kořík, J. Miszczak, and V. Bužek, Quantum parrondo's game with random strategies, *Journal of Modern Optics* **54**, 2275 (2007).
- [13] S. Banerjee, Parrondo's game using a discrete-time quantum walk, *Physics Letters A* **375**, 1553 (2011).
- [14] J. Rajendran and C. Benjamin, Playing a true parrondo's game with a three-state coin on a quantum walk, *Europhysics Letters* **122**, 40004 (2018).
- [15] J. Rajendran and C. Benjamin, Implementing parrondo's paradox with two-coin quantum walks, *Royal Society open science* **5**, 171599 (2018).
- [16] T. Machida and F. A. Grünbaum, Some limit laws for quantum walks with applications to a version of the parrondo paradox, *Quantum Information Processing* **17**, 241 (2018).
- [17] Z. Walczak and J. H. Bauer, Noise-induced parrondo's paradox in discrete-time quantum walks, *Physical Review E* **108**, 044212 (2023).
- [18] Z. Walczak and J. H. Bauer, Parrondo's paradox in quantum walks with three coins, *Physical Review E* **105**, 064211 (2022).
- [19] Z. Walczak and J. H. Bauer, Parrondo's paradox in quantum walks with deterministic aperiodic sequence of coins, *Physical Review E* **104**, 064209 (2021).
- [20] G. Trautmann, C. Groiseau, and S. Wimberger, Parrondo's paradox for discrete-time quantum walks in momentum space, *Fluctuation and Noise Letters* **21**, 2250053 (2022).
- [21] J. W. Lai and K. H. Cheong, Parrondo effect in quantum coin-toss simulations, *Phys. Rev. E* **101**, 052212 (2020).
- [22] J. W. Lai, J. R. A. Tan, H. Lu, Z. R. Yap, and K. H. Cheong, Parrondo paradoxical walk using four-sided quantum coins, *Phys. Rev. E* **102**, 012213 (2020).
- [23] A. Mielke, Quantum parrondo games in low-dimensional hilbert spaces, *preprint arXiv:2306.16845* (2023).
- [24] M. A. Pires and S. M. D. Queirós, Parrondo's paradox in quantum walks with time-dependent coin operators, *Physical Review E* **102**, 042124 (2020).
- [25] D. K. Panda, B. V. Govind, and C. Benjamin, Generating highly entangled states via discrete-time quantum walks with parrondo sequences, *Physica A* **608**, 128256 (2022).
- [26] M. Jan, N. A. Khan, and G. Xianlong, Territories of parrondo's paradox and its entanglement dynamics in quantum walks, *The European Physical Journal Plus* **138**, 65 (2023).
- [27] M. Jan, Q.-Q. Wang, X.-Y. Xu, W.-W. Pan, Z. Chen, Y.-J. Han, C.-F. Li, G.-C. Guo, and D. Abbott, Experimental realization of parrondo's paradox in 1d quantum walks, *Advanced Quantum Technologies* , 1900127 (2020).
- [28] V. Mittal and Y.-P. Huang, Parrondo's paradox in quantum walks with inhomogeneous coins, *Phys. Rev. A* **110**, 052440 (2024).
- [29] Z. Walczak and J. H. Bauer, Parrondo's paradox in quantum walks with different shift operators, *Quantum Information Processing* **23**, 1 (2024).
- [30] G. Kadiri, Scouring parrondo's paradox in discrete-time quantum walks, *Phys. Rev. A* **110**, 022421 (2024).
- [31] T. Hosaka and N. Konno, Parrondo's game of quantum search based on quantum walk, *Quantum Information Processing* **23**, 247 (2024).
- [32] J. W. Lai and K. H. Cheong, Parrondo's paradox from classical to quantum: A review, *Nonlinear Dynamics* , 1 (2020).
- [33] J. J. Ximenes, M. A. Pires, and J. M. Villas-Bôas, Parrondo's effect in continuous-time quantum walks, *Phys. Rev. A* **109**, 032417 (2024).
- [34] J.-P. Allouche and J. Shallit, *Automatic sequences: theory, applications, generalizations* (Cambridge university press, 2003).
- [35] E. Maciá, Alloy quasicrystals: perspectives and some open questions at forty years, *Symmetry* **15**, 2139 (2023).
- [36] M. A. Pires, N. Crokidakis, and S. M. Duarte Queirós, Randomness in ecology: The role of complexity on the Allee effect, *Physica A* **589**, 126548 (2022).
- [37] A. Y. Fernandes, J. A. Hoyos, and A. P. Vieira, Contact process with aperiodic temporal disorder, *Brazilian Journal of Physics* **53**, 84 (2023).
- [38] H. Barghathi, D. Nozadze, and T. Vojta, Contact process on generalized fibonacci chains: infinite-modulation criticality and double-log periodic oscillations, *Physical Review E* **89**, 012112 (2014).
- [39] J.-M. Luck, Parrondo games as disordered systems, *Eur. Phys. J. B* **92**, 1 (2019).
- [40] M. A. Pires, E. P. Pinto, R. N. da Silva, and S. M. Duarte Queirós, Parrondo's effects with aperiodic protocols, *Chaos: An Interdisciplinary Journal of Nonlinear Science* **34**, 123126 (2024).
- [41] P. Ribeiro, P. Milman, and R. Mosseri, Aperiodic quantum random walks, *Phys. Rev. Lett.* **93**, 190503 (2004).
- [42] A. Romanelli, The fibonacci quantum walk and its classical trace map, *Physica A* **388**, 3985 (2009).
- [43] G. Di Molfetta, L. Honter, B. B. Luo, T. Wada, and Y. Shikano, Massless dirac equation from fibonacci discrete-time quantum walk, *Quantum Stud.: Math. Found.* **2**, 243 (2015).
- [44] R. F. S. Andrade and A. M. C. Souza, Discrete-time quantum walks generated by aperiodic fractal sequence of space coin operators, *Int. J. Mod. C* **29**, 1850098 (2018).
- [45] N. Lo Gullo, C. V. Ambarish, T. Busch, L. Dell'Anna, and C. M. Chandrashekar, Dynamics and energy spectra of aperiodic discrete-time quantum walks, *Phys. Rev. E* **96**, 012111 (2017).
- [46] M. A. Pires and S. M. D. Queirós, Quantum walks with sequential aperiodic jumps, *Physical Review E* **102**, 012104 (2020).
- [47] T. K. Bose, Influence of generic quantum coins on the spreading and entanglement in binary aperiodic quantum walks, *Quantum Information Processing* **23**, 102 (2024).
- [48] Z.-J. Li and J. Wang, Single-point position and transition defects in continuous time quantum walks, *Scientific Reports* **5**, 13585 (2015).
- [49] W. Steurer and D. Sutter-Widmer, Photonic and phononic quasicrystals, *Journal of Physics D: Applied Physics* **40**, R229 (2007).
- [50] L. Dal Negro and S. V. Boriskina, Deterministic aperiodic nanostructures for photonics and plasmonics appli-

- cations, *Laser & Photonics Reviews* **6**, 178 (2012).
- [51] A. M. Childs, E. Farhi, and S. Gutmann, An example of the difference between quantum and classical random walks, *Quantum Information Processing* **1**, 35 (2002).
 - [52] R. Zhang, P. Xue, and J. Twamley, One-dimensional quantum walks with single-point phase defects, *Physical Review A* **89**, 042317 (2014).
 - [53] J. P. Keating, N. Linden, J. C. F. Matthews, and A. Winter, Localization and its consequences for quantum walk algorithms and quantum communication, *Physical Review A* **76**, 012315 (2007).
 - [54] E. Agliari, A. Blumen, and O. Mülken, Quantum-walk approach to searching on fractal structures, *Physical Review A* **82**, 012305 (2010).
 - [55] J. A. Izaac, J. B. Wang, and Z. J. Li, Continuous-time quantum walks with defects and disorder, *Physical Review A* **88**, 042334 (2013).
 - [56] C. Benedetti, M. A. Rossi, and M. G. Paris, Continuous-time quantum walks on dynamical percolation graphs, *Europhysics Letters* **124**, 60001 (2019).
 - [57] Z. J. Li, J. A. Izaac, and J. B. Wang, Position-defect-induced reflection, trapping, transmission, and resonance in quantum walks, *Physical Review A* **87**, 012314 (2013).
 - [58] Z.-J. Li and J. Wang, An analytical study of quantum walk through glued-tree graphs, *Journal of Physics A: Mathematical and General* **48**, 355301 (2015).
 - [59] L. I. da S. Teles and E. P. Amorim, Localization in quantum walks with a single lattice defect: A comparative study, *Brazilian Journal of Physics* **51**, 911 (2021).
 - [60] C. Kiumi and K. Saito, Eigenvalues of two-phase quantum walks with one defect in one dimension, *Quantum Information Processing* **20**, 171 (2021).
 - [61] A. Jagannathan, The Fibonacci quasicrystal: Case study of hidden dimensions and multifractality, *Rev. Mod. Phys.* **93**, 045001 (2021).
 - [62] X. Wu and M. Nomura, Mathematically inspired structure design in nanoscale thermal transport, *Nanoscale* **10.1039/D4NR04385E** (2025).
 - [63] M. A. Pires, G. Di Molfetta, and S. M. D. Queirós, Multiple transitions between normal and hyperballistic diffusion in quantum walks with time-dependent jumps, *Scientific Reports* **9**, 1 (2019).

Appendix A: Some exacts results for the binary persistence

In this Appendix we compute the exact Binary Persistence $BP(m)$ of order m for the periodic and random sequences.

1. Periodic sequence

We analyze $BP(m)$ for different values of m in the periodic sequence $S = 01010101\dots$

For $m = 1$, all blocks of length 1 consist of either 0 or 1, so they are trivially identical. Then, $N_{ID}(1) = N_T(1) = \text{length of the sequence}$. Thus, $BP(1) = 1$.

For any $m > 1$, any subsequence of length m will con-

tain both 0s and 1s because the sequence alternates. Example for $m = 3$: possible blocks are 010, 101, which are not identical. Similarly, for larger m , the pattern continues to alternate. Thus, $N_{ID}(m) = 0$ for all $m \geq 2$. Therefore, $BP(m) = 0$.

In summary, for the periodic sequence we obtain

$$BP(m) = \begin{cases} 1 & \text{if } m = 1, \\ 0 & \text{if } m \geq 2. \end{cases} \quad (\text{A1})$$

2. Random sequence

For a binary random sequence with equal probabilities $p(0) = 0.5$ and $p(1) = 0.5$, we obtain:

1. Probability of an all-0 block of length m :

$$P(0_m) = \prod_{i=1}^m p(0) = (0.5)^m \quad (\text{A2})$$

2. Probability of an all-1 block of length m :

$$P(1_m) = \prod_{i=1}^m p(1) = (0.5)^m \quad (\text{A3})$$

3. Probability of either an all-0 or all-1 block (identical block):

$$P_{ID}(m) = P(0_m) + P(1_m) = 2 \times (0.5)^m = (0.5)^{m-1} \quad (\text{A4})$$

In summary, for a sufficiently long sequence, the expected value of $BP(m)$ for a binary random sequence with $p(0) = p(1) = 0.5$ is:

$$BP(m) = \left(\frac{1}{2}\right)^{m-1} \quad (\text{A5})$$

Appendix B: Extra results

Figure 8 shows how the standard deviation of several random sequences is distributed around the average for the interval switching that produces the maximum spreading at time $t = 4000\gamma$.

For this switching interval (which corresponds to the optimal τ for the random protocol, see Figure 4), we observe that all 100 random realizations exhibit enhanced spreading ($\sigma/\sigma_0 > 1$). The mean σ/σ_0 for the random sequences, as well as the values for the other sequences (indicated by vertical lines for their specific values of τ), generally follows the hierarchy of autocorrelation and persistence. Although some individual random sequences can surpass the Rudin–Shapiro case, such events are rare.

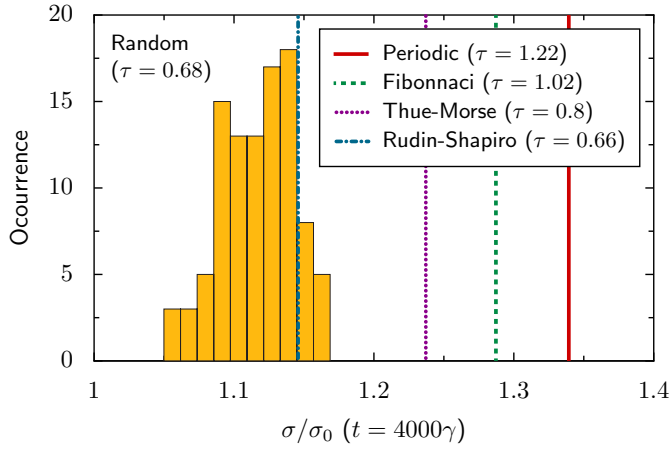


FIG. 8. Histogram of σ/σ_0 for 100 random sequences. The peak of the distribution (the most frequent σ/σ_0 value) is lower than that of the Rudin-Shapiro sequence, although some individual random realizations surpass it. The σ/σ_0 values for the other sequences are indicated by vertical lines for comparison.